Highly correlated hydride ion tracer diffusion in $SrTiO_{3-x}H_x$ oxyhydrides

Xin Liu[1], Tor Svendsen Bjørheim*[,1], Lasse Vines[1], Øystein Slagtern Fjellvåg[1], Cecilie Granerød[1], Øystein Prytz[1], Takafumi Yamamoto[2], Hiroshi Kageyama[2], Truls Norby[1], Reidar Haugsrud*[,1]

[1]Centre for Materials Science and Nanotechnology, University of Oslo, Sem Sælands vei 26, , 0371, Oslo, Norway

[2]Graduate School of Engineering, Kyoto University, Nishikyo–ku, Kyoto 615–8510, Japan

*Corresponding author: torsb@kjemi.uio.no; reidar.haugsrud@smn.uio.no

Abstract

Mixed oxide hydride anion systems constitute a novel class of materials exhibiting intriguing properties such as solid–state hydride ion conduction and fast anion exchange. In this contribution we derive the kinetics of hydride ion transport in a mixed oxide-hydride system, $SrTiO_{3-x}H_x$ through isotope exchange and depth profiling. DFT calculations indicate that migration of H^- to neighboring vacant oxygen lattice sites is fast, but that long-range transport is impeded by slow reorganization of the oxygen sublattice. From measured hydride tracer diffusion coefficients and the correlation factors derived from DFT, we are able to derive the hydrogen self–diffusion coefficients in $SrTiO_{3-x}H_x$. More generally, the explicit description of hydride ion transport in $SrTiO_{3-x}H_x$ through combination of experimental and computational methods reported in this work can be applied to explore anion diffusion in other mixed anion systems.

Introduction

Hydride ion defects have been reported in many main group metal oxides, leading to unintentional n-type conductivity in ZnO, [1-3] but also enabling *e.g.* light-induced insulator-semiconductor transition in Mayenite ($12CaO•7Al_2O_3$). [4-5] In recent years, several transition metal perovskites such as $ATiO_{3-x}H_x$ (A = Ba, Sr and Ca), have been shown to dissolve up to 20% of hydride ions at the expense of oxide ions upon reaction with CaH_2, forming so-called *oxyhydrides.* Such oxyhydrides exhibit solid-state hydride ion conductivity, and fast hydrogen exchange, rendering them potential alternatives to traditional ionic conductors in energy applications and novel catalysts. [4-8] Hydride ion incorporation in *e.g.* $ATiO_{3-x}H_x$ is however accompanied by reduction of Ti, [9-11] inducing semiconducting or metallic behavior, which overshadows any partial hydride ion conductivity. Quantification of the kinetics of hydride ion transport and exchange of these mixed anion systems through electrochemical methods is as such challenging.

So far, the only report of direct measurement of hydride ion conduction is for a series of ionic oxyhydrides, $La_{2-x-y}Sr_{x+y}LiH_{1-x+y}O_{3-y}$ [7] and Ln_2LiHO_3 (Ln = La, Pr and Nd) [12]. Bridge *et al.* [13] probed diffusion of hydride ions in $LaSrCoO_3H_{0.7}$ by using quasielastic neutron scattering (QENS) and reported that hydride ions diffuse through vacant hydride sites with an activation energy of 0.23 ± 0.045 eV. However, the QENS data collection requires few hours at each temperature, which may result in oxyhydride decomposition. Tang *et al.* implemented the Kissinger method to estimate the apparent activation energies of H_2 release and H/D exchange for $BaTiO_{3-x}H_x$ and $LaSrCoO_3H_{0.7}$, trying to link the activation energies to the migration enthalpy of hydride ions. [14] This is, however, an indirect method. In addition, along with several reports, [14-15] they hypothesized the hydride ion migration will be impeded by the oxide ion motion, but this has so far not been shown by any experimental data.

Yajima *et al.*[10] annealed $ATiO_{3-x}H_x$ (A = Ba, Sr, Ca) oxyhydride thin films in deuterium gas followed by characterization by means of secondary ion mass spectrometry (SIMS). It was found that the hydride ions in these oxyhydride films can be exchanged by deuteride ions (D^-), without changing the composition beyond the isotope exchange; the same behavior as reported for powder samples.[10, 16] Accordingly, tracer annealing and depth profiling by SIMS can potentially be applied to investigate the kinetics of hydride ion transport in oxyhydrides.

In the present study, the kinetics of hydride ion transport in $SrTiO_{3-x}H_x$ oxyhydrides is determined by means of isotope exchange followed by SIMS depth profiling on thin films. First principles calculations are furthermore adopted to reveal the mechanisms of hydride ion diffusion and correlation effects by oxide ions on the hydride ion tracer diffusion.

Experimental procedure

$SrTiO_3$ (STO) thin films (~80 nm) were deposited by Pulsed Laser Deposition (PLD) on $(LaAlO_3)_{0.3}(SrAl_{0.5}TaO_3)_{0.7}$ (LSAT) substrates, followed by deposition of a thin (~4 nm) amorphous $LaAlO_3$ (LAO) film to protect the surface of STO films from being over–reduced in the following CaH_2 treatment, yielding a uniform hydride concentration within the STO layer. The deposited films and CaH_2 powder were vacuum–sealed in a Pyrex ampule, and then treated at 530 °C for different reaction times; 1 day, 3 days and 5 days, hereafter denoted as STOH–1, STOH–3 and STOH–5, respectively. The lattice parameters of as–deposited and CaH_2 treated STO films were investigated by thin film X–ray diffraction. The thin–film specimens were annealed in ~800 mbar D_2 (Chemical purity > 99%) at different temperatures. This D_2 pressure was chosen during the tracer measurements since it corresponds to the H_2 pressure forming when annealing CaH_2 in reaction chamber of isotopic exchange. Diffusion profiles were determined by SIMS.

All first principles calculations were conducted using Density Functional Theory (DFT) as implemented in the VASP code. [17-18] The GGA–PBE exchange correlation functional was applied with a Hubbard–U correction (GGA+U) of 4.49 eV to Ti 3d orbitals.[19] The minimum energy path (MEP) for anion migration between two stable configurations was determined by using the climbing–image Nudged Elastic Band (ci–NEB) method.[20-21] Further details of experimental procedures and methodologies are presented in the Supplementary Information (SI-1 section).

Results and discussion

The quality and orientation of the as–deposited and CaH_2 treated STO films were initially investigated by XRD (Figure 1). As only the (00*l*)–reflections are visible in the θ–2θ–scans, it is evident that the films are oriented in the out–of–plane direction, the (00*l*)–direction. ϕ–scans of the (103)–reflections of the substrate and the films (SI–Figure 2) show that the films are oriented

in–plane as well as out–of–plane, giving the epitaxial relationship STO(001)[100]||LSAT(001)[100] with the substrate for the as–deposited and CaH_2–treated films. Reciprocal Space Maps (RSM) of the (103)–reflection are employed to study strain in the films, and RSM of STO and STOH–5 are shown in Figure 1B and 1C, respectively. From the position of the film peaks in $q_{||}$ in the RSM, it is evident that these STO films are strained by the LSAT substrate, and all CaH_2–treated films have the same in–plane lattice parameters. The smaller lattice parameter of the LSAT substrate induces in–plane contraction, making the STO films compressively strained. RSM of STOH–1 and STOH–3 are shown in SI–Figure 3, and the cell parameters of all thin films in this study are summarized in SI–Table 1.

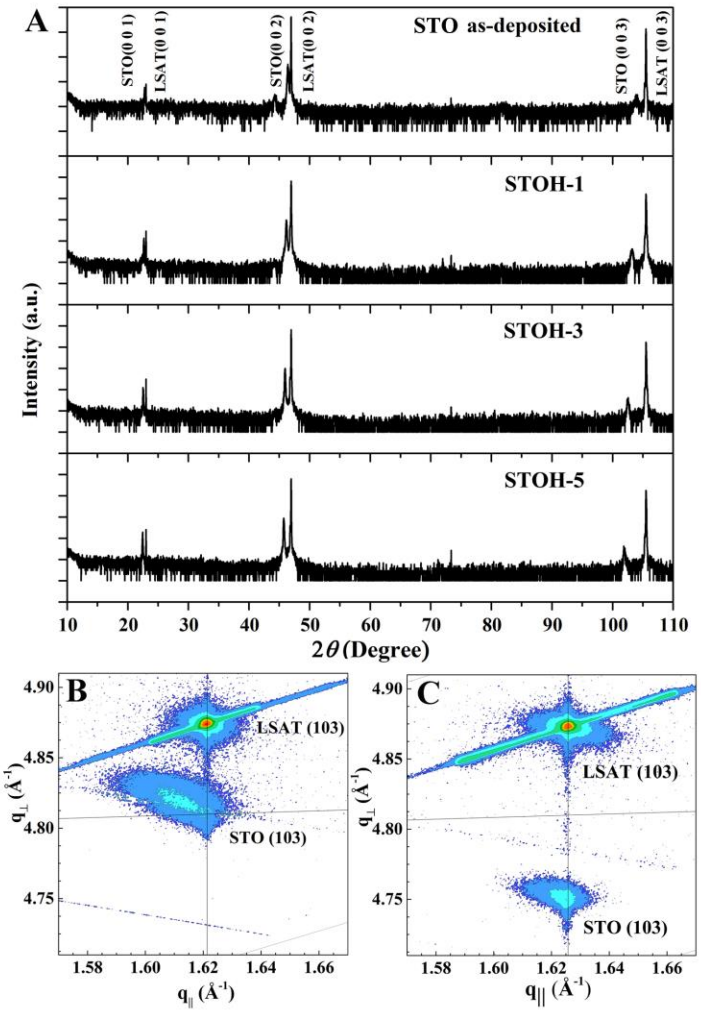

Figure 1. A): θ–2θ scans of STO–as–deposited and CaH_2 treated films. The STO peak shifts towards lower angles, indicating that the cell parameter out–of–plane increases with increased

hydride treatment. B): RSM of the (103)–reflection on STO–as–deposited; C): RSM of the (103)–reflection on STOH–5.

The out–of–plane (*c*–axis) lattice parameter of the as–deposited STO film is 3.920 Å, which is close to the lattice parameter of bulk STO (3.905 Å). Bouily *et al.* reported that the hydride content in $SrTiO_{3-x}H_x$ thin films can be controlled by varying the CaH_2 reaction time: *E.g.*, increasing the exposure time from 1 day to 5 days, the hydride content increases from $x = 0.25$ to $x = 0.45$. [9] Indeed, in our study, we observe the lattice parameter of the STO films increases, suggesting that the hydride ion content is increasing with increased reaction time (as shown in SI–Figure 4). The cell expansion upon hydride ion incorporation is consistent with a previous report on STO powder samples. [16] Considering that our experimental setup and conditions are similar to the previous experimental report, [9] the compositions of STOH–1, STOH–3 and STOH–5 are estimated to be $SrTiO_{2.75}H_{0.25}$, $SrTiO_{2.65}H_{0.35}$ and $SrTiO_{2.55}H_{0.45}$, respectively. RSM results have further shown that the out–of–plane lattice parameter changes on increased CaH_2 reaction time, while the in–plane lattice parameters remain the same due to strain from the substrate.[16] The (00l)–reflections from the LSAT substrate do not shift, hence it may be taken that the substrate is inert and that hydride anions do not dissolve in it.

High resolution Scanning Transmission Electron Microscopy (STEM) images of the STOH–1 film were collected and a representative series of images from the interface region between the STO and LSAT are presented in Figure 2 (STEM images of the STO as–deposited are shown in SI–Figure 5). Figure 2A shows the STO film with a uniform thickness of ~80 nm, with a sharp interface to the LSAT substrate. The STO shows epitaxial growth, and no defects or stacking faults were found in the LSAT or the substrate. Higher magnification imaging shown in Figure 2B reveals an atomically sharp LSAT/STO interface, in good agreement with XRD results that the STO films are strained by the LSAT substrate, as illustrated in Figure 2G. In the STO, Sr is heavier than Ti, and the Sr columns thus appear brighter than Ti columns in STEM mode. Energy dispersive X–ray spectroscopy (EDS) was used to screen the element distribution along the interface, and atomic resolution mappings of selected elements are displayed in Figure 2D. The Sr map shows that the Sr–containing columns are aligned across the interface. The intensity from Sr is slightly lower in the LSAT, whereas these positions are also occupied with La atoms, as seen in the La map. Additionally, Al and Ta maps show that these elements

occur only on the substrate side, and are aligned with the Ti columns in STO. The ideal structure across the interface is illustrated in Figure 2F and the EDS results show that the mapped elements are located at their intended positions. This, along with the STEM images, shows that the STO film is of high quality without observing any grain boundaries. Furthermore, the interface between STO and LAO displayed in Figure 2C shows that the LAO film is amorphous as–grown on the STO film. EDS maps across the LAO film are shown in Figure 2E. Here the La signal mapped within the STO reflects overlap of La and Ti X–ray peaks.

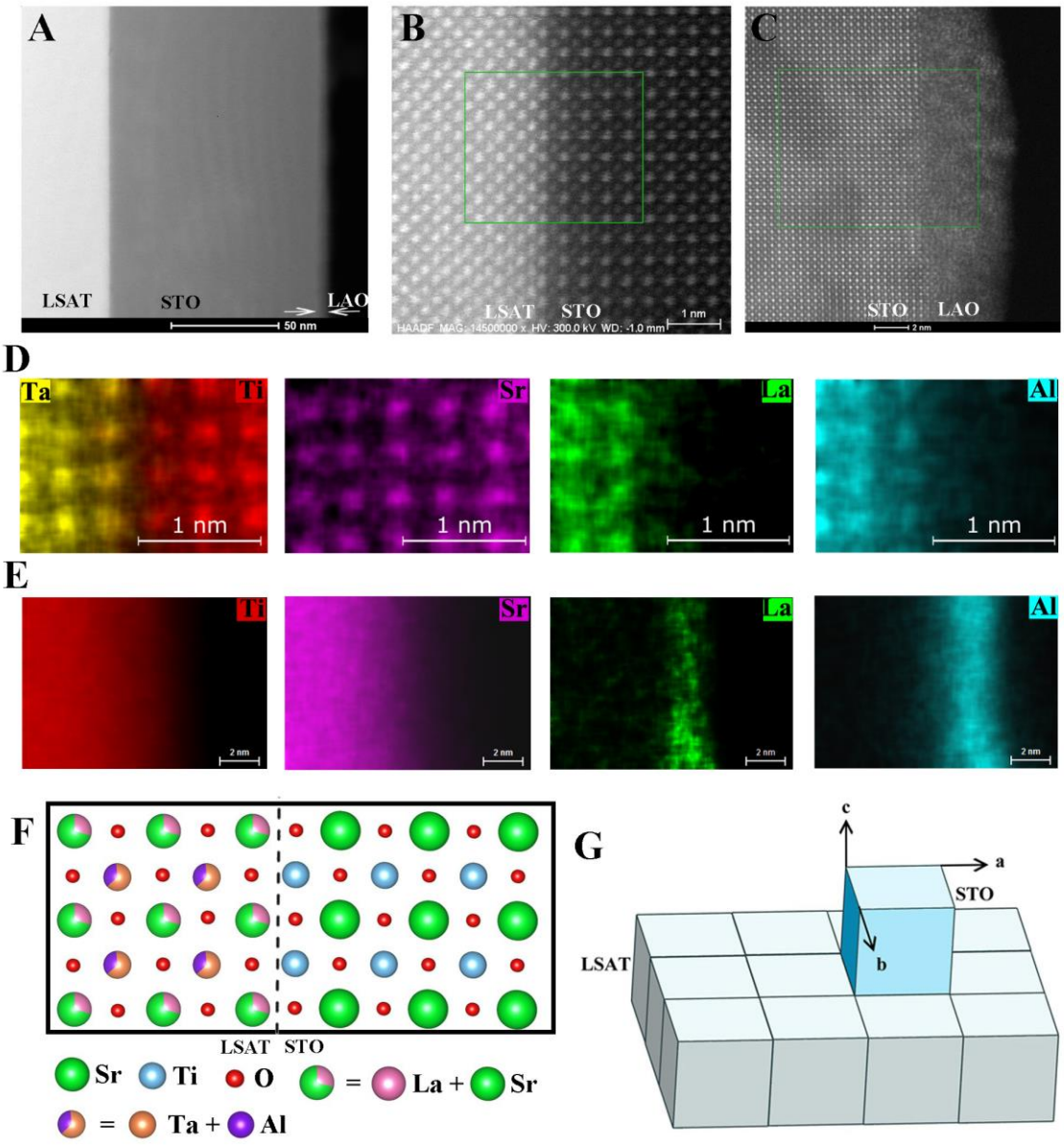

Figure 2. A) STEM HAADF image of thin film STOH–1. B) STEM image of the interface between LSAT substrate and STO, and D) its corresponding EDS mapping images. C) STEM image of the interface between LSAT and LAO, and E) its corresponding EDS images. F) Illustration of interface between LSAT and STO. G) Scheme of STO oriented growth on LSAT.

SIMS depth profiles reveal that H, O, Ti and Sr are uniformly distributed through the thin film except for the surface region (cf. SI–Figure 7A.). Based on TEM investigations, the outer LAO layer is around 4 nm in thickness and corresponds to the surface region with high concentration of hydrogen and low concentration of Sr and Ti. The high concentration of H in the LAO indicates that hydride species are directly taken up by the LAO amorphous film and diffuse through the film to reduce the STO by forming $SrTiO_{3-x}H_x$ oxyhydrides during the CaH_2 treatment. Formation of the oxyhydride is evident by the uniform hydrogen SIMS signal, which has been rationalized by the substitutional hydride ions in the previous study on $ATiO_{3-x}H_x$ (A = Ba, Sr and Ca) oxyhydride thin films, [9, 11] and by that the H concentration is far higher than what expected from H-sources present during PLD film growth. The fact that the hydrogen signal diminishes close to the substrate layer indicates that LSAT is stable during the CaH_2 treatment.

For oxide ion conductors one may utilize isotope annealing followed by SIMS to determine oxygen tracer diffusion properties for the materials. As previously mentioned, a similar approach could in principle be used to determine diffusion data for the hydride ions in oxyhydrides. One major prerequisite during such tracer experiments is that there are no changes in the chemical potential between the two annealing conditions (solely an isotope gradient and no chemical gradient). In the case of oxyhydrides this is challenging to fulfill experimentally, since it requires control of both the hydrogen and oxygen chemical potential under rather unconventional conditions. It is feasible to control the hydrogen activity, but far more difficult with oxygen, since it depends on the impurity level of water vapor in the gas atmospheres and even leakages in the experimental set-up. Moreover, oxyhydrides are vulnerable towards decomposition in humid atmospheres which further complicates the situation (as described in SI-1.1). To illustrate these challenges, we annealed a STOH film in a mixture of ~800 mbar of D_2 gas and 0.1 mbar of $^{18}O_2$. The resulting SIMS profile (cf. SI-Figure 8) shows a clear hydrogen loss and ^{18}O gradient at the surface region, reflecting that even such trace amounts of O_2 gas can oxidize the oxyhydride thin film.

After isotopic exchange under a D_2 activity similar to the H_2 activity (approx. 800 mbar) during CaH_2 annealing, the hydrogen signal (H+D) is essentially constant and identical to the specimen before isotopic exchange (cf. SI-Figure 7B). In addition, the identical oxygen signal after isotopic exchange indicates the no re-oxidation occurs, reflecting the oxygen sublattice is in pseudoequilibrium. This observation is consistent with previous studies, showing that almost complete H/D exchange can be achieved in both $ATiO_{3-x}H_x$ (A= Ba and Sr) bulk and thin film samples without changing the composition of oxyhydrides.[10-11] We therefore believe that performing the D_2 exchange in this way is as close as we can get to pure tracer exchange with essentially no chemical potential driving force affecting the exchange, at least on the time scale of the experiment. The extracted diffusion coefficients as such represent that of tracer diffusion.

Figure 3 displays two deuterium (D) diffusion profiles determined by SIMS depth profiling of STOH–5 specimens annealed in D_2 gas at 450 °C for 11.5 and 21.3 min. Such profiles form the basis for quantifying the hydride ion tracer diffusion coefficients, $D^*_{H_O}$, by solving Fick's second law diffusion equation in semi–infinite medium [22] (details in SI–section 1.3). The penetration depth is clearly larger with increasing reaction time together with the diffusion–type SIMS profiles. The tracer diffusion coefficients extracted from fitting the SIMS profiles in Figure 3 are $1.62 \pm 0.10 \times 10^{-16}$ and $1.01 \pm 0.03 \times 10^{-16}$ cm^2s^{-1} for the longer and shorter diffusion times, respectively. The similar values suggest that the diffusion coefficient is close to independent of the annealing time.

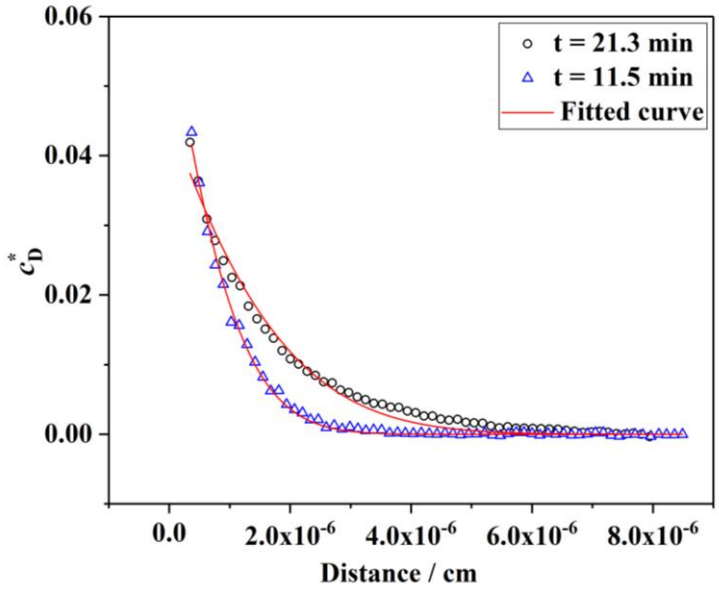

Figure 3. Normalized deuterium fraction, c_{D}^{*} in STOH–5 thin film sample. Sample annealed at 450 °C in $p_{\mathrm{D_2}}$ = 800 mbar for 11.5 and 21.3 min, respectively. The best fits of SI–Eqn. 4 are included as solid lines.

The hydride ion tracer diffusion coefficients extracted are summarized in Figure 4. (All diffusion profiles are summarized in SI–Figure 9 and SI–Table 2.) The specimens with higher hydride concentration, STOH–5 or STOH–3, exhibit similar diffusion coefficients and temperature dependencies. For STOH–1, however, the diffusion coefficients are lower and show almost no temperature dependency. The apparent activation energies of $D_{\mathrm{H_O}}^{*}$ for STOH–3 and STOH–5 by assuming an Arrhenius–type behavior come out as 0.45 ± 0.04 and 0.47 ± 0.03 eV, respectively.

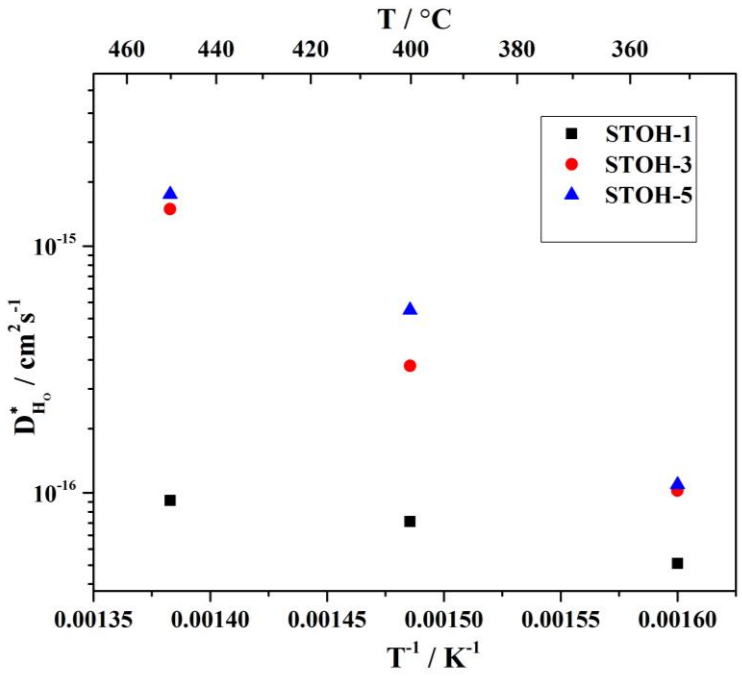

Figure 4. Temperature and composition dependency of the tracer diffusion coefficients $D_{\mathrm{H_O}}^{*}$.

Hydride ions have been suggested to diffuse via a vacancy–mediated mechanism in several oxyhydrides such as $ATiO_{3-x}H_x$ (A = Sr and Ba)[11, 14, 23], $LaSrCoO_3H_{0.7}$[13] and $LaSrLiH_2O_2$ [6-7, 12, 24]. Unlike the anisotropic hydride ion conduction through the metal hydride layer of the latter two oxyhydrides, isotropic transport of both hydride ions and oxide ions occurs in $ATiO_{3-x}H_x$ (A= Sr and Ba). It is then expected that oxide ions and hydride ions will jump with

different activation energies and effective rates into a vacant site, and as such may be assigned individual self–diffusion coefficients and partial ionic conductivities. On the other hand, it is clear that the presumably faster hydride ions for long–range traceable transport, such as in isotope exchange tracer diffusion (giving rise to a tracer diffusion coefficient), will be slowed down by the necessity for random diffusion of vacancies. One may state this in terms of a correlation factor: The hydride ion will jump back to the now empty site that it came from until the vacancy in the meantime has diffused on. If the concentration of hydride ions is small, this has to take place entirely by diffusion of oxide ions – a presumably slower process than for hydride ions. At low hydride ion concentrations this will give rise to a large correlation effect, *i.e.*, a small numerical value for the correlation factor between the tracer and self–diffusion coefficients of hydride ions.

To further study the correlation factor and derive kinetic properties, we have adopted the diffusion model of homogeneous binary alloys given by Manning.[25] In our case, the alloying elements are oxide and hydride ions in an otherwise ternary oxide, but the vacancy mechanism of diffusion on the alloyed sublattice remains the same. Note that we have excluded the possibility for hydride ion migration through interstitial-type mechanisms in the following discussion (see SI–1.5 for a detailed discussion on such mechanisms). The hydride ion tracer diffusion and self–diffusion coefficients can be related through [26]:

$$D^{*}_{\mathrm{H_O}} = f_{\mathrm{H_O}} D_{\mathrm{H_O}} = f_{\mathrm{H_O}} \frac{1}{6} a^2 N x_v \omega_{\mathrm{H_O}} \qquad (1)$$

where a cubic model was adopted by considering that strain of STO in this study is around 1%, which has negligible influence on the oxide ion isotropic transport. [27] a is the jumping distance ($\frac{c}{\sqrt{2}}$, $c \approx 3.92$ Å) and N is the number of nearest neighbor sites which here equals 8. x_v is the site fraction of oxygen vacancies and $\omega_{\mathrm{H_O}}$ represents the jump rate of the hydride ion to its adjacent vacant oxygen site. $f_{\mathrm{H_O}}$ is the correlation factor for the tracer hydride ion diffusion, and essentially holds information about how hydride ion transport is slowed down by the necessity of oxide ion transport in order to move oxygen vacancies. $f_{\mathrm{H_O}}$ can be calculated from the ratio of sufficiently energetic vibrational jump attempts of hydride ions and oxide ions, $\frac{\omega_{\mathrm{H_O}}}{\omega_{\mathrm{O}}}$, through the equations; [26]

$$f_{H_O} = \frac{\frac{2}{1-f}\left(\frac{\omega_{H_O}}{\omega_O} x_{H_O} f_{H_O} + x_O f_O\right)}{2\frac{\omega_{H_O}}{\omega_O} + \frac{2}{1-f}\left(\frac{\omega_{H_O}}{\omega_O} x_{H_O} f_{H_O} + x_O f_O\right)} \quad (2)$$

$$f_O = \frac{\frac{2}{1-f}\left(\frac{\omega_{H_O}}{\omega_O} x_{H_O} f_{H_O} + x_O f_O\right)}{2 + \frac{2}{1-f}\left(\frac{\omega_{H_O}}{\omega_O} x_{H_O} f_{H_O} + x_O f_O\right)} \quad (3)$$

where x_i represents the site fraction of diffusion component i (oxide or hydride ions). f is the correlation factor for the vacancy–mediated diffusion in the pure crystal (f = 0.78 for a cubic lattice with 8 nearest neighbors).

Alternatively, f_{H_O} can be obtained by $\frac{D^*_{H_O}}{D^*_O}$ through the equations in the SI–section 1.4. However, experimental determination of D^*_O is not straightforward since $SrTiO_{3-x}H_x$ would be oxidized in the presence of O_2 or other oxygen–containing atmospheres, leaving out *e.g.* $^{18}O/^{16}O$ isotope exchange. Consequently, we have employed DFT to estimate the jump rate (ω_{H_O} and ω_O) of both hydride ion and oxide ion migration through an oxygen vacant site in $SrTiO_3$, shown in Figure 5.

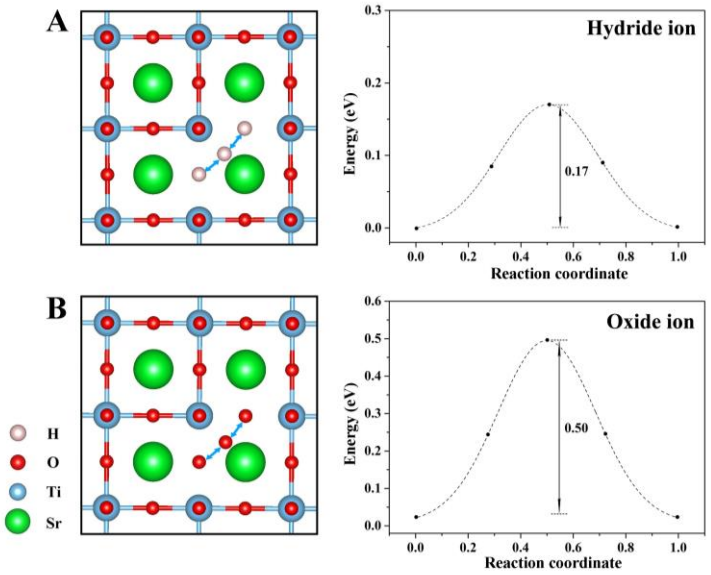

Figure 5. A) Hydride ion and B) oxide ion migration to adjacent vacant oxygen sites, with their associated energy profiles.

We have calculated the energy profile of hydride ion migration to an adjacent vacant site in an oxide ion sublattice, revealing a corresponding migration enthalpy of 0.17 eV, which is slightly lower than that obtained in the QENS study on $LaSrCoO_3H_{0.7}$ (0.23 eV) [13] and our previous computational contribution on $BaTiO_{3-x}H_x$ (0.28 eV) [23]. The difference encountered for the alkaline earth titanates may stem from the smaller unit cell of $SrTiO_3$ (3.968 **Å**) compared to that of $BaTiO_3$ (4.059 **Å**). This has also been reflected in experimental results of oxygen diffusion where the migration enthalpy of oxygen ions in $SrTiO_3$ and $BaTiO_3$ single crystal is determined to be 0.6 [28-29] and 0.7 eV [30], respectively. Notably, our computational results show a migration enthalpy for oxide ion migration in $SrTiO_3$ of 0.50 eV, slightly lower than the experimental value (0.6 eV) [28-29]. The higher activation energy of oxide ion migration compared to that of hydride ion can be rationalized by the charge–state difference.

According to the Eyring reaction rate theory [31], the jump rate can be calculated from the migration enthalpy ΔH_{m} and an effective frequency v^*:

$$\omega_i = v^* \exp\left(\frac{-\Delta H_{\mathrm{m},i}}{k_{\mathrm{B}} T}\right) \qquad (4)$$

where the effective frequency v^* can be calculated based on transition state theory[32]:

$$v^* = \frac{\prod_k^{3T-3} v_k}{\prod_{j=1}^{3T-4} v_j'} \qquad (5)$$

Here, v_k and v_j' are the normal vibrational frequencies at the equilibrium and transition states, respectively, for a system with a number of T atoms and one vacant site. The resulting $\omega_{\mathrm{H_O}}$ and ω_{O} are summarized in SI–Table 2. $\frac{\omega_{\mathrm{H_O}}}{\omega_{\mathrm{O}}}$ is calculated to be 2786, 1764 and 1190 at 350, 400 and 450 °C, respectively, which shows that the jump rate of hydride ions is considerably higher than that of oxide ions, due to the smaller charge and mass and lower migration enthalpy of hydride ions. The correlation factors of hydride ions ($f_{\mathrm{H_O}}$) for different compositions and temperatures are shown in Figure 6A.

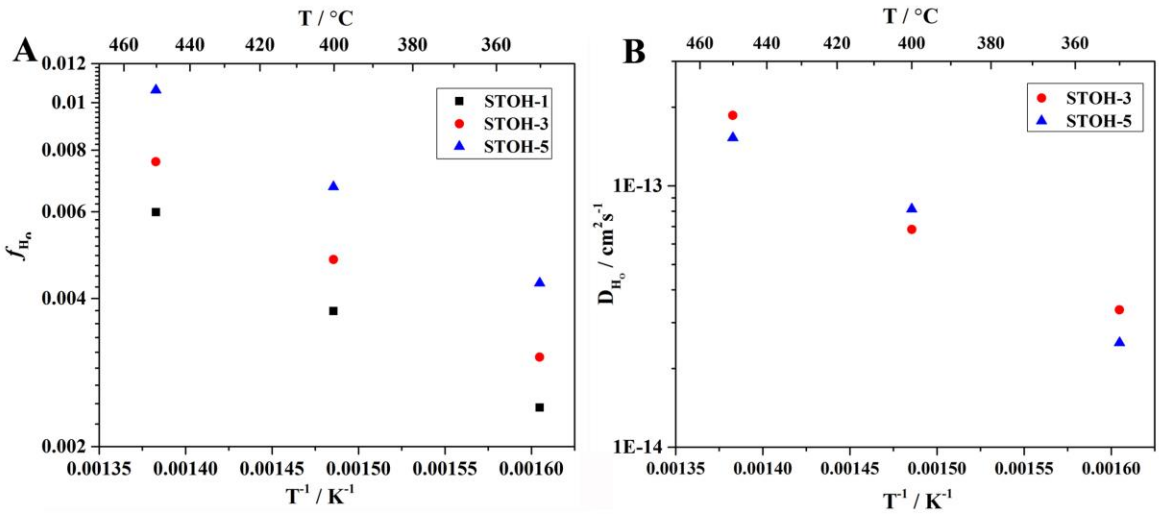

Figure 6. Temperature dependencies of (A) the calculated correlation factors f_{H_O} and (B) self–diffusion coefficients D_{H_O}.

The correlation factor f_{H_O} is orders of magnitude lower than those of, for instance, oxygen tracer diffusion in oxides (f equals 0.78 for face centered cubic structured oxides). This stems from the high jump rate ratio $\frac{\omega_{H_O}}{\omega_O}$ and low site fraction ratio $\frac{x_{H_O}}{x_O}$ in $SrTiO_{3-x}H_x$: after a jump of the hydride ion, it is highly probable that it is followed by a second jump in the reverse direction. The correlation factor f_{H_O} shows a strong temperature dependency (as shown in Figure 6A) stemming from the temperature dependency of $\frac{\omega_{H_O}}{\omega_O}$ which, in turn, reflects the higher activation energy of oxide ions than for hydride ions. Moreover, f_{H_O}shows a compositional dependency. The increasing hydride ion content in the oxyhydride lattice increases the value of f_{H_O}, because the hydride ions have a relatively lower probability to be followed by a reverse jump when another hydride ion can cause the vacancy to diffuse away.

By combining the calculated correlation factors f_{H_O} with the experimental tracer–diffusion coefficients from this study by using Eqn (1), the self–diffusion coefficients (D_{H_O}) are obtained and plotted in Figure 6B. The results of D_{H_O} for STOH–3 and STOH–5 yield activation energies of 0.28 ± 0.05 and 0.30 ± 0.04 eV, respectively, which is similar to the activation energy of hydride ion hopping (0.23 ± 0.045) from the QENS study of $LaSrCoO_3H_{0.7}$. Based on the estimated ω_{H_O} and f_{H_O} from DFT, the site fraction of oxygen vacancies (x_v) can again be

estimated through Eqn. (1) (summarized in SI–Table 2), yielding fractions many orders of magnitude lower than that of hydride ions. The low fraction of vacant anion sites is also reflected by the neutron and synchrotron diffraction study on $SrTiO_{3-x}H_x$ powders. [14, 16] The low concentration of vacant anion sites may reflect that oxyhydride formation proceeds through pure O^{2-}/H^- ion exchange;

$$CaH_2(s) + O_O^{\times} + Ti_{Ti}^{\times} \rightleftharpoons H_O^{\bullet} + Ti_{Ti}^{/} + \frac{1}{2}H_2(g) + CaO\ (s) \qquad (6)$$

As such, the actual $v_O^{\bullet\bullet}$ to $H_O^{\bullet}$ ratio in the reduced oxide can be expected to depend on the applied synthesis and post–annealing conditions, and we do not disregard that materials with significantly higher vacancy concentrations – and consequently – more favorable hydride ion transport properties may be achieved.

Conclusions

Thin films of $SrTiO_{3-x}H_x$ oxyhydrides with various hydride ion contents were produced by treating PLD grown thin $SrTiO_3$ films in CaH_2 for different durations. The hydride ion tracer diffusion coefficients were determined by H/D isotope exchange followed by isotope depth profiling by SIMS. The apparent activation energy of the tracer diffusion coefficients, $D_{H_O}^{*}$, for STOH–3 and STOH–5 are determined to be 0.45 ± 0.04 and 0.47 ± 0.03 eV, respectively. The correlation factors from first principle calculation shows that long-range H^- transport of is impeded by the availability of oxygen vacancies due to slow reorganization of the oxygen sublattice. From these correlation factors and the measured tracer diffusion coefficients, the hydride ion self–diffusion coefficients are obtained, with average activation energies of 0.29 eV. Hence, realization of novel ionic conductors with high hydride ion diffusivity necessitates fast oxygen dynamics, or systems in which the hydride ions migrate by uncorrelated mechanisms. This study as such provides an explicit description of hydride ion transport in oxyhydrides and the methodology can be extended to study anion diffusion in other mixed anion systems.

Acknowledgement

This work is supported by The Faculty of Mathematics and Natural Sciences, University of Oslo via the Strategic Research Initiative and the FOXHOUND project. The calculations were performed on resources provided by UNINETT Sigma2 – the National Infrastructure for High

Performance Computing and Data Storage in Norway. The Research Council of Norway is acknowledged for the support to the Norwegian Center for X–ray Diffraction, Scattering and Imaging (RECX), the Norwegian Center for Transmission Electron Microscopy (NORTEM) and UNINETT Sigma2.This work is also supported by JSPS KAKENHI (Grant Number 16K21724).

References

(1) Janotti, A.; Van de Walle, C. G., Hydrogen multicentre bonds. *Nat. Mater.* **2007,** *6*, 44-7.
(2) Lavrov, E. V.; Börrnert, F.; Weber, J., Photoconductivity and infrared absorption study of hydrogen-related shallow donors in ZnO. *Phys. Rev. B* **2005,** *72*, 085212.
(3) Koch, S. G.; Lavrov, E. V.; Weber, J., Photoconductive Detection of Tetrahedrally Coordinated Hydrogen in ZnO. *Phys. Rev. Lett.* **2012,** *108* (16), 165501.
(4) Hayashi, K.; Sushko, P. V.; Shluger, A. L.; Hirano, M.; Hosono, H., Hydride Ion as a Two-Electron Donor in a Nanoporous Crystalline Semiconductor $12CaO{\cdot}7Al_2O_3$. *J. Phys. Chem. B* **2005,** *109*, 23836-23842.
(5) Hayashi, K.; Matsuishi, S.; Kamiya, T.; Hirano, M.; Hosono, H., Light-induced conversion of an insulating refractory oxide into a persistent electronic conductor. *Nature* **2002,** *419*, 462.
(6) Yamaguchi, S., Large, soft, and polarizable hydride ions sneak around in an oxyhydride. *Science* **2016,** *351*, 1262-1263.
(7) Kobayashi, G.; Hinuma, Y.; Matsuoka, S.; Watanabe, A.; Iqbal, M.; Hirayama, M.; Yonemura, M.; Kamiyama, T.; Tanaka, I.; Kanno, R., Pure H^- conduction in oxyhydrides. *Science* **2016,** *351*, 1314-1317.
(8) Watanabe, A.; Kobayashi, G.; Matsui, N.; Yonemura, M.; Kubota, A.; Suzuki, K.; Hirayama, M.; Kanno, R., Ambient Pressure Synthesis and H^- Conductivity of $LaSrLiH_2O_2$. *Electrochemistry* **2017,** *85*, 88-92.
(9) Bouilly, G.; Yajima, T.; Terashima, T.; Yoshimune, W.; Nakano, K.; Tassel, C.; Kususe, Y.; Fujita, K.; Tanaka, K.; Yamamoto, T.; Kobayashi, Y.; Kageyama, H., Electrical Properties of Epitaxial Thin Films of Oxyhydrides $ATiO_{3-x}H_x$ (A = Ba and Sr). *Chem. Mater.* **2015,** *27*, 6354-6359.
(10) Yajima, T.; Kitada, A.; Kobayashi, Y.; Sakaguchi, T.; Bouilly, G.; Kasahara, S.; Terashima, T.; Takano, M.; Kageyama, H., Epitaxial Thin Films of $ATiO_{3-x}H_x$ (A = Ba, Sr, Ca) with Metallic Conductivity. *J. Am. Chem. Soc.* **2012,** *134*, 8782-8785.
(11) Kobayashi, Y.; Hernandez, O. J.; Sakaguchi, T.; Yajima, T.; Roisnel, T.; Tsujimoto, Y.; Morita, M.; Noda, Y.; Mogami, Y.; Kitada, A.; Ohkura, M.; Hosokawa, S.; Li, Z.; Hayashi, K.; Kusano, Y.; Kim, J. e.; Tsuji, N.; Fujiwara, A.; Matsushita, Y.; Yoshimura, K.; Takegoshi, K.; Inoue, M.; Takano, M.; Kageyama, H., An oxyhydride of $BaTiO_3$ exhibiting hydride exchange and electronic conductivity. *Nat. Mater.* **2012,** *11*, 507-511.
(12) Iwasaki, Y.; Matsui, N.; Suzuki, K.; Hinuma, Y.; Yonemura, M.; Kobayashi, G.; Hirayama, M.; Tanaka, I.; Kanno, R., Synthesis, crystal structure, and ionic conductivity of hydride ion-conducting Ln_2LiHO_3 (Ln = La, Pr, Nd) oxyhydrides. *J. Mater. Chem. A* **2018,** *6*, 23457-23463.
(13) Bridges, C. A.; Fernandez-Alonso, F.; Goff, J. P.; Rosseinsky, M. J., Observation of Hydride Mobility in the Transition-Metal Oxide Hydride $LaSrCoO_3H_{0.7}$. *Adv. Mater.* **2006,** *18*, 3304-3308.
(14) Tang, Y.; Kobayashi, Y.; Shitara, K.; Konishi, A.; Kuwabara, A.; Nakashima, T.; Tassel, C.; Yamamoto, T.; Kageyama, H., On Hydride Diffusion in Transition Metal Perovskite Oxyhydrides Investigated via Deuterium Exchange. *Chem. Mater.* **2017,** *29* (19), 8187-8194.
(15) Kutsuzawa, D.; Hirose, Y.; Chikamatsu, A.; Nakao, S.; Watahiki, Y.; Harayama, I.; Sekiba, D.; Hasegawa, T., Strain-enhanced topotactic hydrogen substitution for oxygen in $SrTiO_3$ epitaxial thin film. *Appl. Phys. Lett.* **2018,** *113*, 253104.
(16) Sakaguchi, T.; Kobayashi, Y.; Yajima, T.; Ohkura, M.; Tassel, C.; Takeiri, F.; Mitsuoka, S.; Ohkubo, H.; Yamamoto, T.; Kim, J. e.; Tsuji, N.; Fujihara, A.; Matsushita, Y.; Hester, J.; Avdeev, M.; Ohoyama, K.; Kageyama, H., Oxyhydrides of $(Ca,Sr,Ba)TiO_3$ Perovskite Solid Solutions. *Inorg. Chem.* **2012,** *51*, 11371-11376.
(17) Perdew, J. P.; Burke, K.; Ernzerhof, M., Generalized Gradient Approximation Made Simple. *Phys. Rev. Lett.* **1996,** *77*, 3865-3868.
(18) Kresse, G.; Furthmüller, J., Efficient iterative schemes for *ab initio* total-energy calculations using a plane-wave basis set. *Phys. Rev. B* **1996,** *54*, 11169-11186.
(19) Zhang, J.; Gou, G.; Pan, B., Study of Phase Stability and Hydride Diffusion Mechanism of $BaTiO_3$ Oxyhydride from First-Principles. *J. Phys. Chem. C* **2014,** *118*, 17254-17259.
(20) Henkelman, G.; Uberuaga, B. P.; Jónsson, H., A climbing image nudged elastic band method for finding saddle points and minimum energy paths. *J. Chem. Phys.* **2000,** *113*, 9901-9904.
(21) Henkelman, G.; Jónsson, H., Improved tangent estimate in the nudged elastic band method for finding minimum energy paths and saddle points. *J. Chem. Phys.* **2000,** *113*, 9978-9985.
(22) Crank, J., The Mathematics of Diffusion, 2nd edn. *The Mathematics of Diffusion, 2nd edn* **1975**, p 60.
(23) Liu, X.; Bjorheim, T. S.; Haugsrud, R., Formation and migration of hydride ions in $BaTiO_{3-x}H_x$ oxyhydride. *J. Mater. Chem. A* **2017,** *5*, 1050-1056.

(24) Liu, X.; Bjorheim, T. S.; Haugsrud, R., Defects formation and their effects on hydride ion transport properties in a series of K_2NiF_4-type oxyhydrides. *J. Mater. Chem. A* **2018,** *6*, 1454-1461.
(25) Manning, J. R., *Diffusion kinetics for atom in crystals*. 1968.
(26) Philibert, J., *Atom movements diffusion and mass transport in solids*. **1968**, p 184-187.
(27) AL-Hamadany, R.; Goss, J. P.; Briddon, P. R.; Mojarad, S. A.; O'Neill, A. G.; Rayson, M. J., Impact of tensile strain on the oxygen vacancy migration in $SrTiO_3$: Density functional theory calculations. *J. Appl. Phys.* **2013,** *113*, 224108.
(28) De Souza, R. A.; Metlenko, V.; Park, D.; Weirich, T. E., Behavior of oxygen vacancies in single-crystal $SrTiO_3$: Equilibrium distribution and diffusion kinetics. *Phys. Rev. B* **2012,** *85*, 174109.
(29) De Souza, R. A., Oxygen Diffusion in $SrTiO_3$ and Related Perovskite Oxides. *Adv. Funct. Mater.* **2015,** *25*, 6326-6342.
(30) Kessel, M.; De Souza, R. A.; Martin, M., Oxygen diffusion in single crystal barium titanate. *Phys. Chem. Chem. Phys.* **2015,** *17*, 12587-12597.
(31) Eyring, H., The Activated Complex in Chemical Reactions. *J. Chem. Phys.* **1935,** *3*, 107-115.
(32) Vineyard, G. H., Frequency factors and isotope effects in solid state rate processes. *J. Phys. Chem. Solids* **1957,** *3*, 121-127.